Three-Dimensional Nuclear Magnetic Resonance Structures of Mouse Epidermal Growth Factor in Acidic and Physiological pH Solutions†,‡

Daisuke Kohda and Fuyuhiko Inagaki*

Department of Molecular Physiology, Tokyo Metropolitan Institute of Medical Science, 18-22, Honkomagome 3-chome, Bunkyo-ku, Tokyo 113, Japan

Received March 27, 1992; Revised Manuscript Received July 23, 1992

ABSTRACT: The three-dimensional structures of epidermal growth factors (EGF) previously reported were all in acidic solutions (pH 2.0–3.2), at which pHs EGF cannot bind to the receptor. Here we studied the structure of mouse EGF at pH 6.8, where EGF is physiologically active, and compared it with the structure at pH 2.0 by CD and NMR. From pH dependence of CD spectra and a comparison between the chemical shifts of the proton resonances at pH 6.8 and 2.0, the conformations at two pHs were found to be nearly identical except for the C-terminal tail region. The three-dimensional structures at pH 6.8 and 2.0 were determined independently by a combination of two-dimensional ^{1}H NMR and simulated annealing calculations using the program XPLOR. The calculations were based on 261 distance constraints at pH 6.8 and 355 distance and 24 torsion angle constraints at pH 2.0. The conformational difference of the C-terminal domain (residues 33–50) was detected between the two structures, which were supported by CD and the chemical shift comparison. The positions of the side chains of Leu47, Arg48, Trp49, and Trp50 are changed probably by the effect of the deprotonation of Asp46. Considering the fact that Leu47 is essential in EGF binding to the receptor, this conformational difference may be important in receptor recognition.

Epidermal growth factor (EGF)[1] and type α transforming growth factor (TGFα) are small peptide hormones which promote cell proliferation (Carpenter & Cohen, 1979, 1990). EGF and TGFα interact with the same specific receptor competitively with similar affinity, and the binding to the receptor induces a conformational change of the extracellular domain of the EGF receptor (Greenfield et al., 1989). Subsequently the ligand-induced conformational change results in receptor oligomerization [Ullrich & Schlessinger (1990) and references therein]. In the oligomerized state the cytoplasmic domains of the receptors are adjacent enough to phosphorylate each other by an intermolecular mechanism (Honegger et al., 1990), which enhances the tyrosine kinase activity of the receptor. After the kinase activation, the oligomers of the EGF–receptor complexes form clusters over clathrin-coated pits and then they are endocytosed within clathrin-coated vesicles (Pastan & Willingham, 1981). During transfer into endosomal vesicles and lysosomes, EGF is proteolytically processed from its C-terminus (Matrisian et al., 1984; Planck et al., 1984). The pH of the solution is neutral (ca. pH 7.4) in intercellular space where EGF binds to the receptor and slightly acidic (ca. pH 5) in intracellular vesicles where EGF is cleaved and dissociates from the receptor (Tycko & Maxfield, 1982).

The determination of three-dimensional structures of proteins with a molecular weight up to 10 000 has been established by the combination of the sequential assignment method developed by Wüthrich and his co-workers (Wüthrich, 1986) and various programs for structure determination: DISGEO (Havel & Wüthrich, 1985); DADAS/DISMAN (Braun & Go, 1985); XPLOR (MSI, Waltham, MA); DSPACE (Hare Research, Inc., Bothell, WA); and GROMOS (van Gunsteren & Berendsen, 1982). We and other researchers published the sequential assignments of human, mouse, and rat EGFs (Cooke et al., 1990; Kohda & Inagaki, 1988;[2] Montelione et al., 1988; Mayo et al., 1989). Kohda et al. (1988) reported the backbone chain fold of mEGF based on mechanical modeling, and Cooke et al. (1987) and Montelione et al. (1987, 1992) reported the computer-based three-dimensional structures of human EGF and mouse EGF (mEGF), respectively. All the pHs used were 2.0–3.2, which are much more acidic than physiological pHs, 5–7.4, because heavy precipitation of mouse and human EGFs in the pH range 3.5–6.5 makes the NMR measurements difficult at physiological pH. Massagué (1983) reported the pH dependence of mouse EGF binding to the receptors in placenta and A431 cell membranes. The binding of mEGF to the receptors in both types of membranes was maximal between pH 7 and 9, 50% at about pH 6, and 0% below pH 5. This prompted us to investigate the structural comparison between mEGF at acidic and physiological pHs.

In the present study we measured the NMR spectra of mEGF at pH 6.8 and assigned all the observable resonances to specific protons using a combination of the sequential assignment method (Wüthrich, 1986) and two-dimensional NMR pH titration method (Kohda et al., 1991). On the basis of the assignments, we analyzed the NOESY spectra and collected interproton distance data. The three-dimensional structure of mEGF at pH 6.8 was determined by the simulated

† This research was supported by grants (to D.K. and F.I.) from the Ministry of Science, Education, and Culture of Japan and from the Human Frontier Science Program Organization (to F.I.).

‡ The coordinates of the structures reported in this paper have been deposited in the Brookhaven Protein Data Bank (entries 1EPG, 1EPH, 1EPI, and 1EPJ).

* To whom correspondence should be addressed.

[1] Abbreviations: CD, circular dichroic; DQF-COSY, double-quantum-filtered correlation spectroscopy; EGF, epidermal growth factor; mEGF, mouse EGF; HOHAHA, homonuclear Hartmann–Hahn spectroscopy; NOE, nuclear Overhauser effect; NOESY, NOE spectroscopy; RMS, root-mean-square; RMSD, RMS deviation; TGFα, type α transforming growth factor; XPLOR-UP, XPLOR utility programs; YASAP, yet another simulated annealing protocol; ⟨ph2⟩, the final set of 10 structures at pH 2.0; ⟨ph7⟩, the final set of five structures at pH 6.8; ph2m, the mean structure at pH 2.0; ph7m, the mean structure at pH 6.8.

[2] Two chemical shift values previously reported in this reference were misprinted: Pro4 C$^\beta$H 2.82 → 2.32 and Cys42 NH 7.30 → 7.80.

0006-2960/92/0431-11928$03.00/0

annealing calculation using XPLOR. In parallel, the three-dimensional structure of mEGF at pH 2.0 was calculated in the same way and was compared with that at pH 6.8. We found that the both structures are almost identical except for a minor difference in the C-terminal tail region (Leu47–Trp50) of mEGF.

MATERIALS AND METHODS

mEGF from submaxillary glands of adult male mice was purified as described (Kohda & Inagaki, 1988).

CD Measurements. CD spectra were recorded on a JASCO J-600 spectropolarimeter with a 5-mm path length cell at room temperature. Eight scans were accumulated. mEGF was dissolved in distilled water at a concentration of 0.082 mg/mL for the wavelength range of 200–250 nm and 0.36 mg/mL for the range of 240–310 nm. We used an extinction coefficient of 3.09 (1 mg/mL, 1 cm) at 280 nm to determine the concentration of mEGF (Taylor et al., 1972). The pH of the CD sample was adjusted by addition of HCl and NaOH and directly measured by inserting a glass electrode into the CD cell. The mean residue ellipticity of mEGF is based on an average residue molecular weight of 114.

NMR Measurements. mEGF was dissolved at 6 mM in 99.95% ^2H_2O or in 90% ^1H_2O/10% ^2H_2O. pH values given are direct pH-meter readings measured at 25 °C with a Radiometer PHM86. The pH value of the sample was 2.8 when the lyophilized EGF powder was dissolved in distilled water. The pH was adjusted to pH 2.0 or 6.8 by addition of ^{2}HCl and NaO^{2}H. No extra salt was added to the samples. To avoid precipitation near the isoelectric point, p*I* 4.6 (Matrisian et al., 1984), the pH of the sample was raised rapidly by addition of a little excess NaO^{2}H and readjusted to pH 6.8 with ^{2}HCl. The mEGF solution at pH 6.8 was a little turbid with a small amount of precipitation. Microcells, BMS-005 purchased from Shigemi, Japan, were used to reduce the sample volume to 0.15 mL (Takahashi & Nagayama, 1988).

^{1}H NMR spectra were recorded on a 500-MHz Jeol JNM-GX500 spectrometer at a probe temperature of 28 °C. Chemical shifts were measured from the internal standard of sodium 2,2-dimethyl-2-silapentane 5-sulfonate. DQF-COSY spectra (Rance et al., 1983), HOHAHA spectra (45-ms mixing time; Bax & Davis, 1985), and NOESY spectra (80- and 200-ms mixing time; Jeener et al., 1979; Macura et al., 1981) were recorded in the phase-sensitive mode (States et al., 1982). A DQF-COSY spectrum for reading $^3J_{NH\alpha}$ was recorded with 512 × 4096 data points, and all other two-dimensional spectra were recorded with 512 × 2048 data points with a spectral width of 6000 Hz. Water resonance was suppressed by selective irradiation during relaxation delay. For measurement of NOESY, water resonance was suppressed by the DANTE pulse (Zuiderweg et al., 1986) or by replacing the last 90° pulse in the sequence by a jump-return pulse (Plateau & Gueron, 1982). A total of 64–128 scans were accumulated for each t_1 with a relaxation delay of 1.5 s. The digital resolution was 5.9 Hz/point (3.0 Hz for reading $^3J_{NH\alpha}$) in both dimensions by zero-filling in the t_1 dimension. A phase-shifted sine function was applied for both t_1 and t_2 dimensions in the case of DQF-COSY and a Lorentz–Gauss function was applied in other cases.

Distance Constraints from NOESY. Interproton distance constraints at pH 2.0 and 6.8 were derived from NOE cross-peak intensities in the NOESY spectra recorded in ^1H_2O and ^2H_2O with a mixing time of 80 ms. An estimate of the peak intensities was obtained by counting the number of contour levels at the peak maximum. The peak intensities in ^2H_2O NOESY were adjusted to those in ^1H_2O using common cross peaks observed in both NOESYs. Peak intensity versus interproton distance was then calibrated making reference to known distances (Wüthrich, 1986): sequential $d_{\alpha N}$ ranges from 2.2 to 3.6 Å, particularly in β-sheet, $d_{\alpha N}$ = 2.2 Å. Since NOE intensity corresponding to $d_{\alpha N}$ was attenuated by a rapid exchange of amide protons with solvent at neutral pH, we used only $d_{\alpha N}$ corresponding to a slowly exchanging amide proton as a reference distance at pH 6.8 and checked it by using $d_{\alpha\alpha}(ij)$ = 2.3 Å between opposite residues on the neighboring antiparallel β-strands. The translation of peak intensity to distance was made on the basis of a relation of (NOE intensity) $\propto$ (distance)$^{-6}$. The relation between NOE and distance is only approximate owing to various factors: isolated spin-pair approximation and internal motions, etc. Thus, the following interproton distances were used to divide NOEs into four groups with upper-bound constraints of 2.5, 3.0, 3.5, and 4.0 Å. The lower-bound distance constraints were set at 1.8 Å for all constraints. For cross peaks involving methyl groups, an additional 0.5 Å per methyl group was added to the upper-bound distance (Clore et al., 1987).

Torsion Angle Constraints from DQF-COSY. The coupling constants $^3J_{NH\alpha}$ were determined for a number of residues in DQF-COSY spectra recorded in ^1H_2O at pH 2.0 (Marion & Wüthrich, 1983). The smallest apparent value of $^3J_{NH\alpha}$ in pH 2 solution was about 4 Hz. Correction was taken into account for cancellation effects due to large line widths (Neuhaus et al., 1985). These coupling constants were used to estimate torsion angles ϕ to be constrained in the range −140° to −100° (>10 Hz) or −160° to −80° (>8 Hz) or −90° to −40° (<5.5 Hz) (Kline et al., 1988). In pH 6.8 solution, no meaningful coupling constants were obtained due to the large line widths.

Other Constraints. Additional distance constraints were obtained from disulfide bonds and hydrogen bonds. mEGF contains three disulfide bonds: Cys6–Cys20, Cys14–Cys31, and Cys33–Cys42 (Savage et al., 1973). A disulfide bond was treated as one distance constraint between the two sulfur atoms of which target values are set to 2.02 ± 0.02 Å. A hydrogen bond was treated as two distance constraints, NH_i–O_j and N_i–O_j, whose target values are set to 1.8 ± 0.5 and 2.8 ± 0.5 Å, respectively.

Simulated Annealing Calculations. Energy minimization and molecular dynamics calculations were made using the program XPLOR (version 2.1, MSI, Waltham, MA) on a Personal Iris 35 (Silicon Graphics Inc., Mountain View, CA). Determination of the three-dimensional structures of proteins from interproton distance constraints and torsion angle constraints is to find a global minimum of a nonlinear target function. XPLOR makes use of Newton's equations of motion for this purpose. The target function has the form

$$F_{total} = F_{bond} + F_{angle} + F_{impr} + F_{repel} + F_{NOE} + F_{tor}$$

where F_{bond} and F_{angle} describe the covalent energy terms for maintaining correct bond lengths and bond angles, respectively. F_{impr} describes energy involving chirality and planarity. F_{repel} describes a repulsion term for preventing unduly close contacts of atoms. F_{NOE} and F_{tor} describe square-well potentials for introducing penalties when the interproton distances or torsion angles deviate from the acceptable value ranges. Detailed definitions are given by Clore et al. (1986) and Brünger (1990).

XPLOR is not a simple program but rather an interpreter of a program language adapted for restrained molecular

dynamics. We used some tutorial programs in the XPLOR manual (Brünger, 1990) with slight modifications. Initial structures were generated by the program randomphipsi.inp using random ϕ and ψ angles with peptide bonds and side chains in an extended conformation and perfect covalent geometry. The program sa.inp, alias YASAP, was used to carry out simulated annealing calculation. YASAP uses a similar but more robust simulated annealing protocol than that used in the hybrid distance geometry-simulated annealing protocol (Nilges et al., 1988). In addition to the tutorial programs, we made some new XPLOR programs for analyses of the calculated structures and UNIX shell programs that invoke these XPLOR programs. We call them XPLOR-UP (XPLOR utility programs). These utility programs greatly increase the efficiency of the calculations and analyses. For instance, a C-shell program run_yasap automatically generates parameter files containing sequentially changing random seeds and invokes sequentially RANDOMPHIPSI and YASAP for each parameter file to produce, for example, 100 structures. In the present version of XPLOR (version 2.1), the nbfix command for adjusting the van der Waals parameters for the sulfur–sulfur interaction in a disulfide bridge does not function. Hence, after the restrained dynamics at 1000 K and just before cooling, a disulfide bridge is connected with a covalent bond with an appropriate patch command.

Analyses of the Computed Structures. Analyses of structures were carried out with XPLOR-UP, and displaying and plotting of structures were carried out with QUANTA (version 3.2, MSI, Waltham, MA) on an Iris 4D/70G. Cartoon drawings of protein structures were generated by the program RIBBON (Priestle, 1988) in the program PAP (QCPE 594, by T. Callahan, University of Minnesota). For quantitative assessment of the convergence of the calculations, a partial sum

$$F_3 = F_{\text{repel}} + F_{\text{NOE}} + F_{\text{tor}}$$

was computed for each structure. The structures with the smallest F_3 values were selected as computationally converged structures. Percentage of retained structures against total calculations was low (2–10%) in the present calculations partly because we did not use the metric matrix distance geometry method to produce roughly folded intermediate structures. It should be noted here that the metric method commonly used by NMR researchers does not include a process called metrization and hence gives a problem of limited sampling of conformational space (Metzler et al., 1989; Kuszewski et al., 1992). Another reason is that the yield of convergence varies significantly depending on the folding nature of proteins. From our experience over 10 protein calculations, EGF is one of the most difficult proteins for NMR structure determination. For quantitative comparisons of different structures, minimum RMS deviations (RMSDs) were calculated for the backbone atoms (N, C^{α}, C′) or the heavy atoms of a specified range of residues. A mean structure was obtained by averaging the coordinates of the structures that are superimposed in advance with respect to the best converged structure. We excluded residues 1 and 51–53 during the superposition due to the absence of NOEs other than intraresidue and sequential ones. Because such an averaged structure was poor in geometry, it was subjected to a restrained Powell minimization: this comprises 200 cycles with the soft van der Waals radii reduced by a factor of $s = 0.25$, 200 cycles with $s = 0.5$, and 800 cycles with $s = 0.8$ (Clore et al., 1986). The final coordinates were obtained by fitting to the mean structure for the backbone atoms of residues 2–50 for pH 2.0 structures and residues 2–22 + 29–50 for pH 6.8 structures. RMSDs per residue were calculated between the individual final structures and the mean structures.

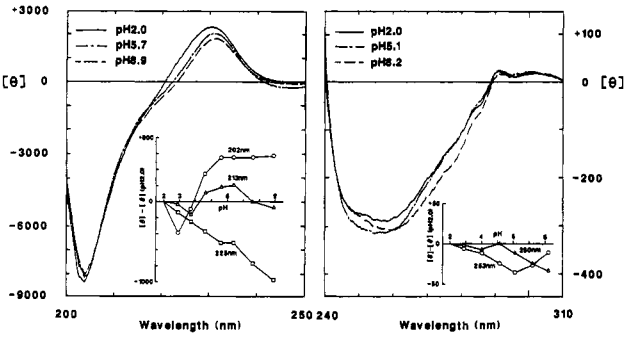

FIGURE 1: CD spectra (mean residue ellipticity, deg·cm²/dmol) of mouse EGF at various pHs. Insets show the pH dependence of $[\theta]$ at 202 nm (aperiodic structure), at 213 nm (β structure), and at 225, 253, and 280 nm (aromatics and disulfides). A difference between $[\theta]$ at a given pH and $[\theta]$ at pH 2.0 was plotted as a function of pH.

RESULTS

pH Dependence of CD Spectra. Figure 1 shows the CD spectra of mEGF in the pH range between 2 and 9. The spectra below 220 nm, arising mainly from the peptide bonds, show no major changes. The negative strong dichroic band at 202 nm is characteristic of aperiodic structure and the shoulder band at 213 nm corresponds to β structure (Taylor et al., 1972; Holladay et al., 1976). Side-chain chromatophores mainly contribute to the spectra above 220 nm. A positive band at 230 nm and negative bands at 240–290 nm have contributions from aromatics and disulfide bridges. They sensitively reflect local conformations around them but show only small changes. Thus the conformation of mEGF does not change greatly in the pH range 2–9. However, minor but significant changes are also seen around pH 4 and 7 in plots of pH versus $[\theta] - [\theta](\text{pH } 2.0)$ (Figure 1, insets), suggesting that minor conformational changes occur as the ionizable groups deprotonate.

Sequence-Specific Resonance Assignment. We previously reported the sequence-specific resonance assignment of mEGF at pH 2.0 (Kohda & Inagaki, 1988). Here we made the sequence-specific resonance assignment at pH 6.8 mainly using the sequential assignment method. The first step of the sequential assignment was to identify spin systems in DQF-COSY and HOHAHA spectra. The spin system identification in the HOHAHA spectrum (45-ms mixing time) was easy by making reference to the HOHAHA spectra at pH 2.0. Then these identified spin systems were connected by sequential NOEs in the NOESY spectrum (200-ms mixing time). Again this was straightforward with reference to the NOESY spectra at pH 2.0. Forty-four residues involving at least one sequential NOE connectivity were unambiguously assigned. At neutral pHs, however, the exchange rates of some amide protons with the solvent water were too fast for NMR observation. In the fingerprint region of the DQF-COSY spectrum in ^1H_2O at pH 6.8, 40 cross peaks were observed; this equals 70% of the number of expected cross peaks. Since the disappearance of amide proton resonances interrupted the sequential walk along the amino acid sequence, the remaining nine residues were only tentatively assigned at this stage by chemical shift comparison between pH 6.8 and 2.1. Definite assignments of these residues were obtained by the two-dimensional NMR pH titration method (Kohda et al., 1991). We measured 12 HOHAHA spectra in ^2H_2O in the pH range from 1.5 to 9.

Table I: Structural Statistics[a]

	⟨ph2⟩	ph2m	⟨ph7⟩	ph7m
average RMS deviations from experimental distance constraints (Å) [pH 2.0, 355; pH 6.8, 261]	0.113 ± 0.003	0.112	0.124 ± 0.002	0.119
no. of distance constraint violations >0.5 Å	1∼3	1	2∼4	2
max violation (Å)	0.82	0.62	0.75	0.73
average RMS deviations from experimental dihedral constraints (deg) [pH 2.0, 24; pH 6.8, 0]	5.7 ± 1.1	4.6		
no. of dihedral constraint violations >20°	0∼1	0		
F_{NOE}[b] (kcal·mol^{-1})	227.2 ± 10.1	224.4	201.9 ± 9.8	185.5
F_{tor}[b] (kcal·mol^{-1})	12.5 ± 4.6	7.61		
F_{repel}[b] (kcal·mol^{-1})	100.3 ± 6.8	98.8	112.3 ± 9.9	105.2
E_{L-J}[c] (kcal·mol^{-1})	−147.2 ± 8.5	−133.5	−148.2 ± 10.9	−156.0
average RMS deviations from idealized geometry:				
bonds (Å) [807]	0.008 ± 0.0003	0.008	0.008 ± 0.0000	0.008
angles (deg) [1430]	2.43 ± 0.02	2.41	2.49 ± 0.02	2.45
impropers[d] (deg) [399]	1.59 ± 0.17	1.53	1.58 ± 0.07	1.43

[a] ⟨ph2⟩ and ⟨ph7⟩ refer to the final sets of the simulated annealing structures at pH 2.0 and 6.8, respectively; the ph2m and ph7m refer to the mean structures obtained by restrained minimization of the averaged coordinates of ⟨ph2⟩ and ⟨ph7⟩, respectively. The number of specified constraints is given in brackets. [b] The value of the square-well NOE potential, F_{NOE}, is calculated with a force constant of 50 kcal·mol^{-1}·Å^{-2}. The value of the square-well torsion angle potential, F_{tor}, is calculated with a force constant of 50 kcal·mol^{-1}·rad^{-2}. The value of the repel term, F_{repel}, is calculated with a force constant of 4 kcal·mol^{-1}·Å^{-4} with the van der Waals radii scaled by a factor of 0.8 of the standard values used in the CHARMm empirical function (Brooks et al., 1983). [c] E_{L-J} is the Lennard–Jones van der Waals energy calculated with the CHARMm empirical energy function (Brooks et al., 1983), which was not included in the simulated annealing calculations. [d] The improper torsion term is used to maintain the planar geometries and chiralities.

The sequence-specific resonance assignments of the remaining residues were accomplished by tracing the shifts of the cross peaks. It should be noted that the assignments at pH 6.8 were completely independent of the assignments at pH 2.0, even though the data at pH 2.0 were quite helpful. These two methods cross-checked the assignments of many proton resonances. A summary of the assignments for mEGF at pH 6.8 is given in Table SI as supplementary material.

Differences of the Chemical Shifts between pH 2.0 and 6.8. Figure 8 shows a comparison between the chemical shifts observed at pH 2.0 and 6.8. The closed bars represent proton resonances of residues having a group that ionizes in the pH range 2–9: Asn1 having an α-amino group; Asp11, Glu24, Asp27, Asp40, Asp46, Glu51, and Arg53 having α-, β-, or γ-carboxyl groups; and His22 having an imidazole group. All these resonances but one (Arg53 C$^{\gamma}$H) move to upfield by −0.05 to −0.4 ppm as pH increases. Almost all other resonances of the residues without ionizable groups show shifts as small as +0.05 to −0.1 ppm. There are some resonances that show significant shifts (shown by hatched bars). These shifts alone could give some insight into the mEGF conformations, but they should be interpreted by reference to the three-dimensional structure of mEGF (see Discussion).

Constraints for Simulated Annealing Calculation. We collected NOE cross peaks from NOESYs in ^1H_2O and ^2H_2O. A short mixing time of 80 ms was used to reduce the effects of spin diffusion. For intraresidue cross peaks, only the NH–X type was collected, where X denotes protons other than amide protons. The intensities of the cross peaks were then translated into upper limits of distance constraints by the calibration described in Materials and Methods. In preliminary calculations, several upper-bound constraints showed systematic violations greater than 0.5 Å. Thus, in the final calculations, these upper-bound constraints were relaxed by 0.2–0.5 Å for taking account of spin diffusion effects: nine intraresidue constraints were increased by 0.2 Å and six interresidue constraints by 0.5 Å for the set at pH 2.0, and three interresidue constraints were increased by 0.5 Å for the set at pH 6.8. Hydrogen bonds between an amide proton and a carbonyl oxygen of the backbone were inferred from slow amide proton exchange rates and characteristic local NOE patterns. Eight interstrand hydrogen bonds were identified: Met21 NH–Thr30 CO, Met21 CO–Thr30 NH, Val19 NH–Asn32 CO, Val19 CO–Asn32 NH, Val34 NH–Tyr37 CO, Val34 CO–Tyr37 NH, Ser38 NH–Thr44 CO, and Ser38 CO–Thr44 NH at both pHs.

With additional constraints from the three disulfide bonds in mEGF, a total of 355 distance constraints at pH 2.0 and 261 distance constraints at pH 6.8 were identified as listed in Table SII as supplementary material. These numbers of NOEs are rather fewer than those expected for a protein of similar size. This is partly because we omitted intraresidue NOEs other than NH–X type and probably because EGF consists of two structural domains between which only a few NOEs were observed. The difference of the total NOE numbers at the two pHs was ascribed to the attenuation of NOE cross peaks involving amide protons due to a rapid exchange with the solvent water at the neutral pH. Aggregation in neutral solution may also cause signal broadening that reduced the observable number of NOE cross peaks. In summary, 145 distance constraints are unique to the set at pH 2.0 and 51 to that at pH 6.8. The remaining 210 distance constraints are common to both sets; among them 133 having identical upper limits and 77 have different ones. The numbers of NOEs involving only nonexchangeable protons are almost the same for both pHs (97 at pH 2.0 and 86 at pH 6.8). Moreover, the weakest cross peaks in the NOESY spectra were found to correspond to the same distance, ca. 3.5 Å at both pHs, considering the $d_{\alpha N}$ maximum distance of 3.6 Å. Thus the quality of the NOESY spectra at pH 2.0 and 6.8 is nearly equal. The interresidue distance constraints are summarized as a diagonal plot (Figure S1 in supplementary material). The overall distributions of NOEs are similar, indicating the same backbone topology at two pHs.

The coupling constants $^3J_{NH\alpha}$ were collected from DQF-COSY spectra recorded in ^1H_2O at pH 2.0. Torsion angle constraints around ϕ were derived from the coupling constant as described in Materials and Methods. A total of 24 torsion angle constraints are listed in Table SIII as supplementary material. No torsion angle constraints were used for pH 6.8 calculations owing to the large line widths of the proton resonances at neutral pH, which prevented us from estimating the coupling constants.

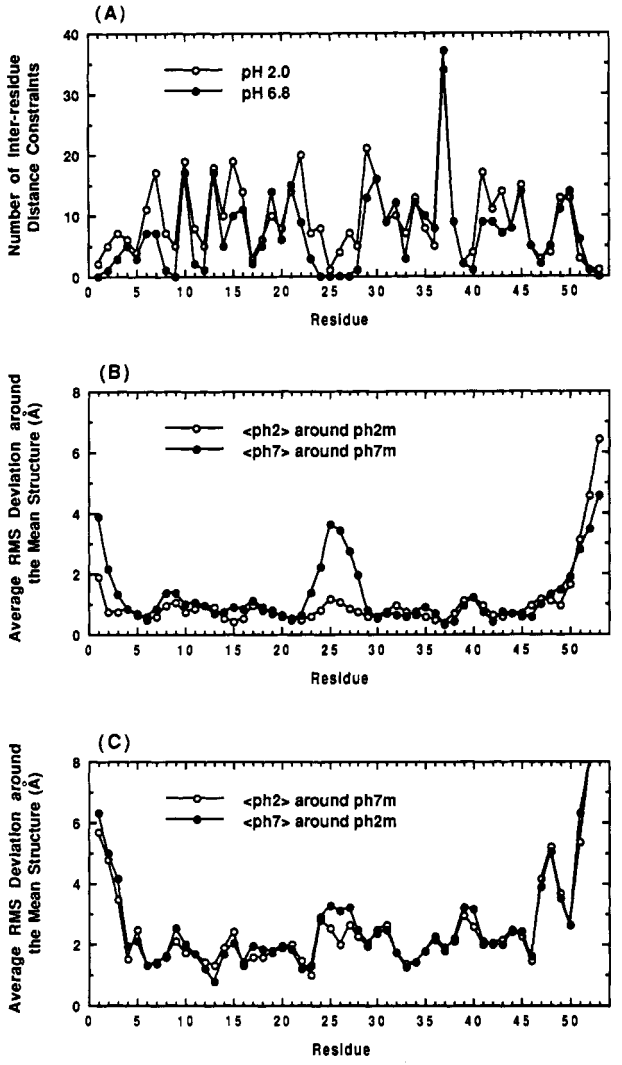

FIGURE 2: (A) Plot of the total number of interresidue distance constraints (interresidue NOEs, disulfide bonds, hydrogen bonds) per residue as a function of residue number. All constraints appear twice, once for each residue number of pairs. The open circles represent the number of constraints per residue at pH 2.0, and the closed circles are at pH 6.8. (B) Plot of the average values of the backbone RMSD per residue as a function of residue number. Individual final structures were fitted to the mean structure for the backbone atoms of residues 2–50. The open circles represent the average values of RMSD per residue between the individual converged structures at pH 2.0 and their mean structure, and the closed circles are at pH 6.8. (C) Same as (B) except that the mean structures were used mutually. The terms ⟨ph2⟩, ⟨ph7⟩, ph2m, and ph7m are defined in Table I.

Simulated Annealing Calculation. A total of 150 calculations were carried out with XPLOR using YASAP protocol for the structure determination of mEGF at pH 2.0 and 250 calculations for that at pH 6.8, starting from randomly generated initial structures. We selected 10 structures at pH 2.0 and five structures at pH 6.8, on the basis of the criterion of the smallest residual energy values of $F_3 = F_{repel} + F_{NOE} + F_{tor}$. Absence or a small number of distance violations greater than 0.5 Å and torsion angle violations greater than 20° was another important criterion (Table I). Small RMS deviations of bonds from idealized geometry (typically <0.010 Å) ensure good geometry of the final structures. We refer to these final structures as ⟨ph2⟩ and ⟨ph7⟩. After fitting to the best converged structure for residues 2–50, the final structures, ⟨ph2⟩ and ⟨ph7⟩, were averaged separately and restrained-minimized to give mean structures at pH 2.0 and 6.8, respectively. We use the terms ph2m and ph7m to refer to the mean structures. The structural statistics for ⟨ph2⟩, ph2m, ⟨ph7⟩, and ph7m are summarized in Table I.

Figure 2A shows the number of *interresidue* distance constraints per residue plotted as a function of the residue number. The overall distributions are similar to each other for the two pHs. However, no interresidue distance constraints are seen in the region of residues 24–27 at pH 6.8 mainly because of the disappearance of amide protons of these residues at the neutral pH. Figure 2B shows the average RMS deviations from the mean structure per residue as a function of the residue number. In the final structures at pH 6.8, large RMS deviations at residues 23–28 are seen. It simply reflects the absence of the interresidue distance constraints in this region (Figure 2A). Thus we excluded residues 23–28 in the superposition of the final structures ⟨ph7⟩ to the mean structure at pH 6.8. In Figure 3A, the best 10 structures at pH 2.0 have been superimposed for pairwise minimum RMSDs with the mean structure for the backbone atoms of residues 2–50. Figure 3B shows the best five structures at pH 6.8 superimposed in a similar manner but for residues 2–22 + 29–50. The backbone superpositions of the N-terminal domain (residues 1–32) and the C-terminal domain (33–53) at pH 2.0 and 6.8 are shown in Figure S2 in supplementary material. The superpositions including side-chain heavy atoms are shown in Figure 4 for pH 2.0 and Figure 5 for pH 6.8. The residues used for fitting were 2–32 and 33–50 for pH 2.0 and 2–22 + 29–32 and 33–50 for pH 6.8. The average and standard deviation values of RMSDs about the mean structures are summarized in Table II for various residue ranges and atom selections.

DISCUSSION

We and other researchers have determined the backbone conformations of EGFs by means of NMR (Cooke et al., 1987; Montelione et al., 1987, 1992; Kohda et al., 1988). The pH values of the NMR sample solutions had to be kept as low as pH 2.0–3.2 to obtain NMR spectra of good quality. Thus, it is consequent to investigate whether the three-dimensional structure in neutral pH solution is identical to that in acidic pH solution. The pH dependence of CD spectra suggested the global tertiary structure of mEGF maintained in the pH range between 2 and 9, but small conformational changes were induced by the deprotonation of the ionizable groups (Figure 1). To investigate the conformational differences in detail, we determined the three-dimensional structure of mEGF at pH 6.8 by means of NMR and compared it with the structure independently determined at pH 2.0.

Our previous structure at pH 2.1 was based on manual model building (Kohda et al., 1988) and checked by a preliminary calculation with the program DADAS/DISMAN (unpublished results). Here we calculated the three-dimensional structures of mEGF at pH 2.0 and 6.8 using the program XPLOR. The 10 final structures of mEGF at pH 2.0 are shown in Figure 3A. They are very similar to our previous mechanical model. The structural features have been described in detail by us and other researchers mainly on the basis of NOEs (Montelione et al., 1986, 1987, 1992; Carver et al., 1986; Cooke et al., 1987; Kohda et al., 1988). Here the simulated annealing calculation of the pH 2.0 structures exhibits a good structural convergence (Figures 3A and 4 and Table II), and so we can describe the backbone structure of mEGF at acidic pH on the basis of the backbone torsion angles ϕ and ψ. Ramachandran plots (Ramachandran et al., 1963) for residues 2–49 of the final structures are shown in Figure

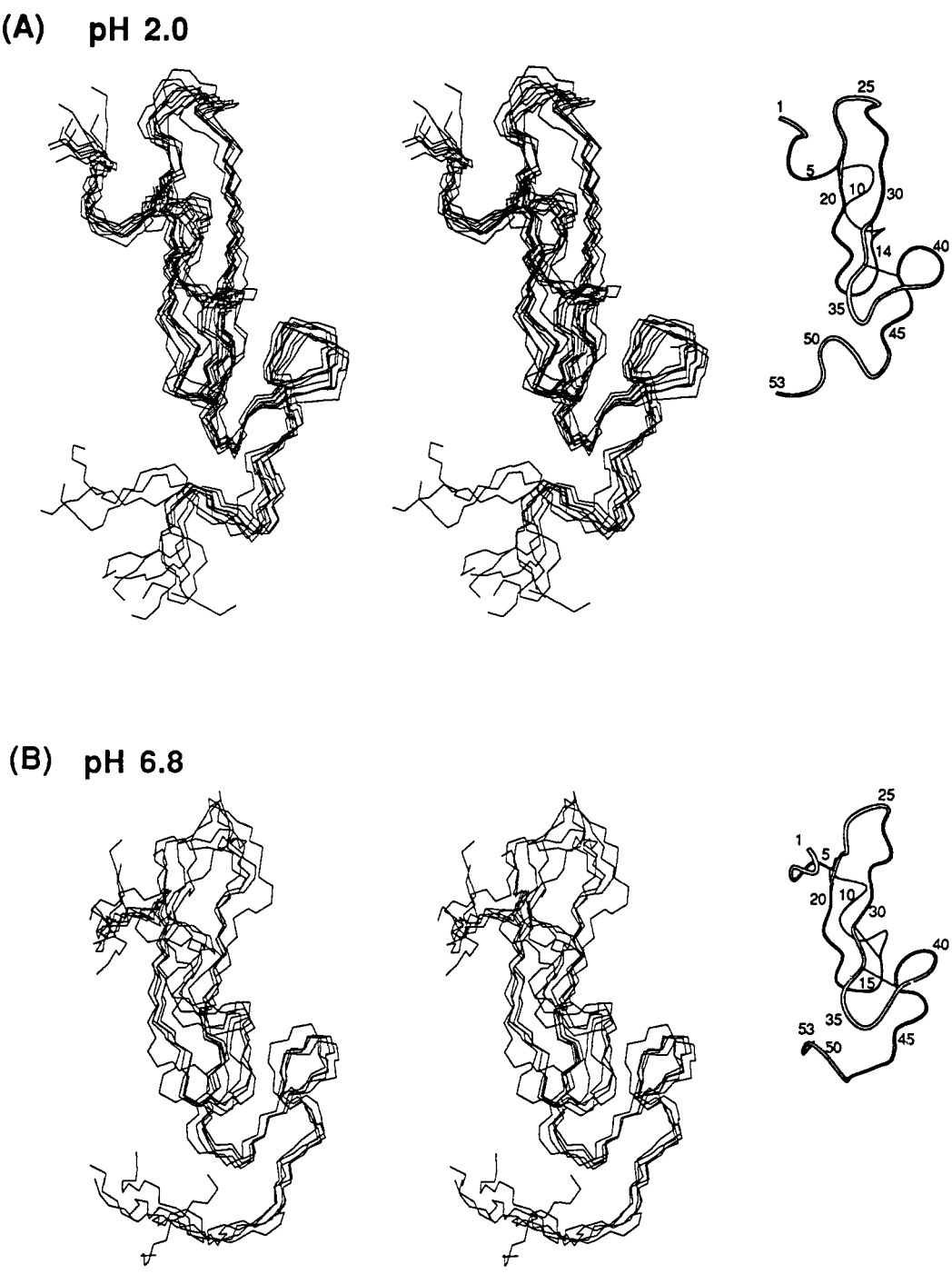

FIGURE 3: (A) Stereoview of a superposition of the backbone (N, C^{α}, C′) atoms of the 10 final XPLOR structures at pH 2.0 best-fitted to their mean structure for the backbone atoms of residues 2–50. (B) Same as (A) for the five final XPLOR structures at pH 6.8 best-fitted to their mean structure for the backbone atoms of residues 2–22 + 29–50. One Ångstrom unit corresponds to 1.75 mm. The insets show the backbone folds with residue numbers.

S3 in supplementary material. ϕ–ψ plots for each residue are also shown in Figure S4.

Mouse EGF consists of two structural domains. The N-terminal domain (Asn1–Asn32) contains an antiparallel β-sheet structure (Val19–Ile23/Ser28–Asn32) to which a third strand (Ser2–Pro4) attaches antiparallel but loosely (Figure 3A). The β-sheet structure may be extended by two residues (Gly18–Ile23/Ser28–Cys33) as stated by Montelione et al. (1987). The third β strand Ser2–Pro4 may be also extended by three residues (Ser2–Pro7) though no opposite strand exits. These three β-strands are connected by two tight turns (Leu15–Gly18 and Glu24–Asp27) and a helixlike structure (Ser8–Cys14). The side chains of Pro7, Tyr10, Tyr13, His22, and Tyr29 probably with Tyr3 form a hydrophobic core in the N-terminal domain (Figure 4A). The C-terminal domain (Cys33–Arg53) contains a short antiparallel β-sheet (Tyr37–Ser38/Thr44–Arg45), one tight turn (Val34–Tyr37), one left-handed loop (Gly39–Gln43), and a tail structure (Asp46–Arg53). The β-strand Thr44–Arg45 may extend in an extended conformation by two residues (Thr44–Leu47) though no opposite strand exists. The segment Arg48–Trp50 takes a folded conformation, which defines a second hydrophobic cluster formed by the side chains of Val34, Ile35, Tyr37, Trp49, and Trp50 and probably with Leu47 (Figure 4B). The residues Asn1 and Glu51–Arg53 are not well defined as compared with other regions, implying some flexibility in solution. The types of tight turns can be recognized from the ϕ and ψ values of residues at position 2 and 3 of the tight turns (Richardson,

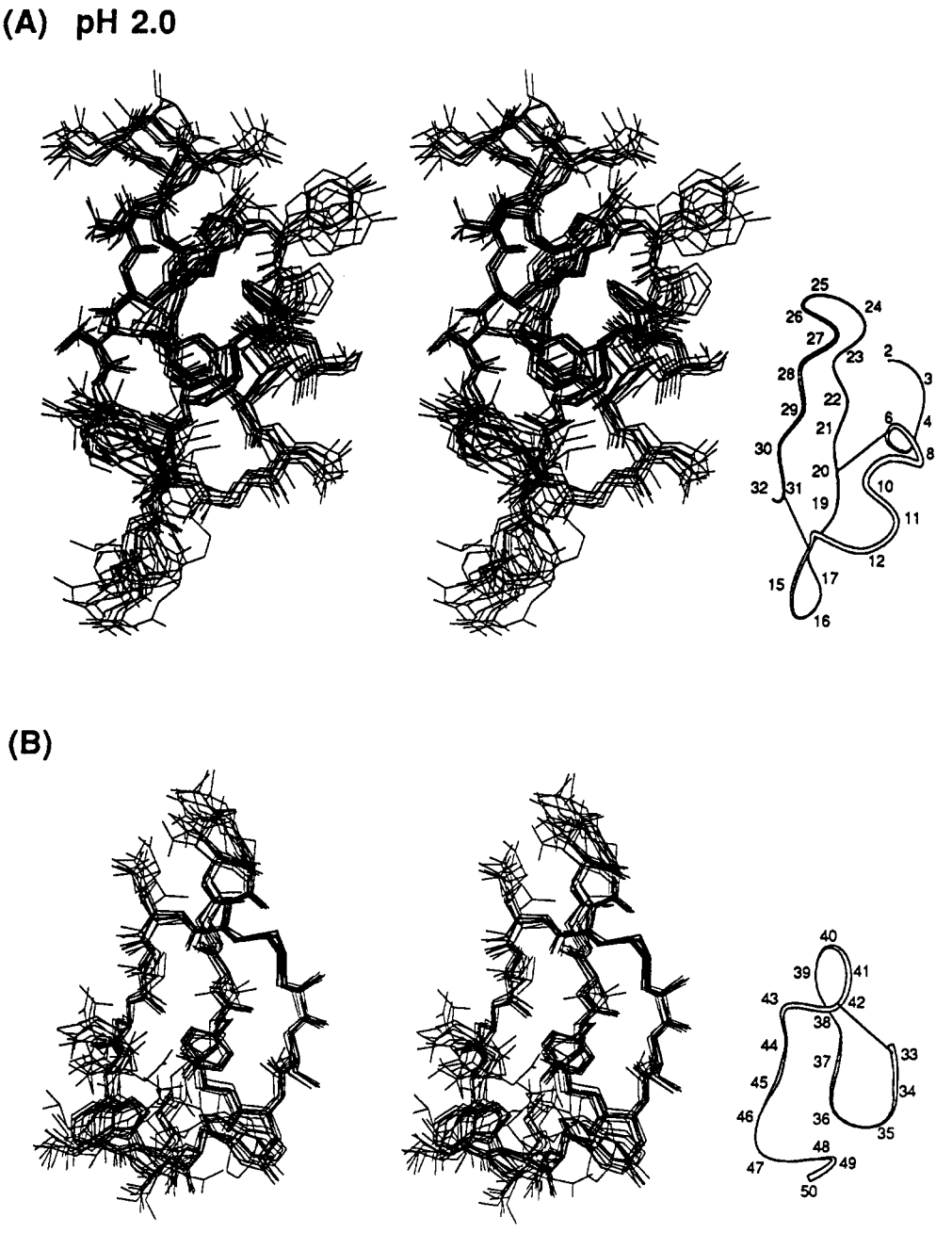

FIGURE 4: (A) Stereoview of a superposition of the heavy atoms of the N-terminal domain, residues 2–32, of the 10 final XPLOR structures at pH 2.0 best-fitted to their mean structure for the heavy atoms of residues 2–32. (B) Same as (A) for the C-terminal domain, residues 33–50, best-fitted for the heavy atoms of residues 33–50. The disulfide bonds are drawn in thick lines. One Angstrom unit corresponds to 2.45 mm. The insets show the backbone fold with residue numbers.

1981). The tight turn Leu15–Gly18 is type I′, Glu24–Asp27 is type I, and Val34–Tyr37 is type II. The segment Cys6–Ser9 may be assigned to a type Ib tight turn. The classification was, however, not very obvious because the ϕ and ψ values were somewhat outside of the typical ranges. In the present calculations, no refinement was applied to the final XPLOR structures. The incorporation of van der Waals and electrostatic potentials into the total energy function will improve the Ramachandran plot.

Figure 3B shows the five XPLOR structures at pH 6.8. The Ramachandran plots are shown in Figures S3 and S4. In Figure 3A,B, the structures at both pHs clearly represent the same global fold of the polypeptide backbone. Thus, the structural features described above for the pH 2.0 structure can be applied to the pH 6.8 structure. However, the CD experiment showed that there were small but appreciable conformational changes around pH 4 and 7. The conformational change around pH 7 caused by the deprotonation of the N-terminal α-amino group has been described in detail using the 2D pH titration method (Kohda et al., 1991). A detailed description of the conformational change around pH 4 was impossible at that time. Here we can do it by comparing the two NOE-based structures at different pHs determined independently. As shown in Figures 3A and 4, the mEGF structure at pH 2.0 shows a structural convergence good enough to discuss the conformation including the side-chain orientations. RMSDs including all heavy atoms are about 1.0 Å for each domain (Table II and Figure S2). Figures 3B and 5 show the superpositions at pH 6.8. The C-terminal domain at pH 6.8 has a small RMSD of 1.2 Å, again enough to describe the side-chain conformation (Table II). In contrast, the N-terminal domain is not well-defined, in particular around residue His22. This is due to disappearance of NOE cross peaks involving the resonances of His22 ring protons in a

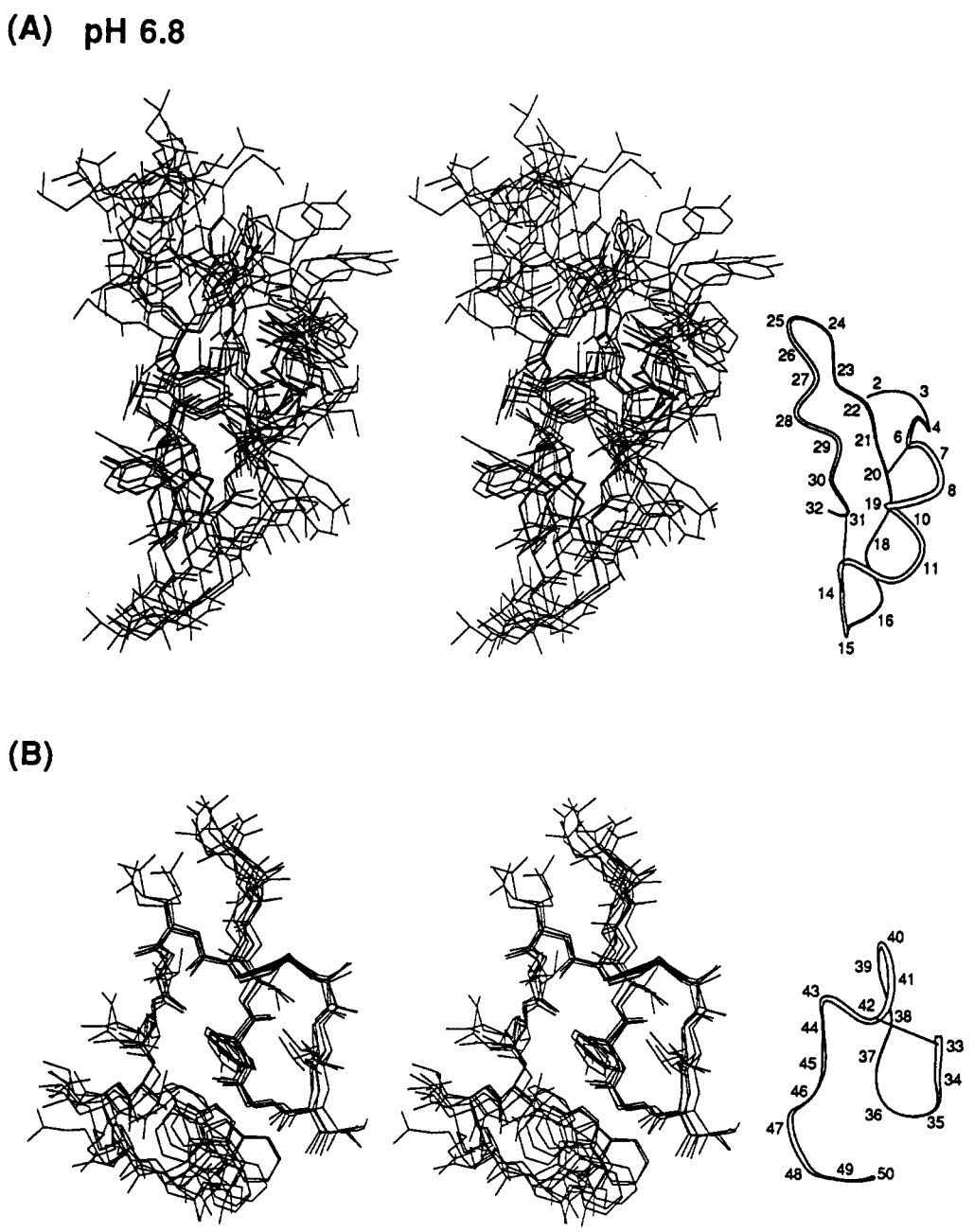

FIGURE 5: (A) Stereoview of a superposition of the heavy atoms of the N-terminal domain, residues 2–32, of the five final XPLOR structures at pH 6.8 best-fitted to their mean structure for the heavy atoms of residues 2–22 + 29–32. (B) Same as (A) for the C-terminal domain, residues 33–50, best-fitted for the heavy atoms of residues 33–50. The disulfide bonds are drawn in thick lines. One Angstrom unit corresponds to 2.45 mm. The insets show the backbone fold with residue numbers.

Table II: RMS Differences of ⟨ph2⟩ and ⟨ph7⟩ around the Mean Structures[a]

	RMSDs (Å)	
atom selection and range	⟨ph2⟩ around ph2m	⟨ph7⟩ around ph7m
backbone (N, C^{α}, C)		
2–50	0.87 ± 0.29	1.00 ± 0.37[b]
2–32	0.65 ± 0.16	0.86 ± 0.25[b]
33–50	0.40 ± 0.14	0.53 ± 0.16
heavy atoms		
2–50	1.24 ± 0.29	1.47 ± 0.41[b]
2–32	0.99 ± 0.15	1.26 ± 0.20[b]
33–50	0.99 ± 0.24	1.19 ± 0.31

[a] The terms ⟨ph2⟩ and ⟨ph7⟩ are defined in Table I. [b] Excluding residues 23–28 due to the absence of interresidue NOEs (Figure 3A).

half-protonated state at pH 6.8 and amide resonances of residues Glu24–Asp27 due to a rapid exchange with the solvent water at neutral pH (Figure 2). In principle, two structures should have the same quality to be compared to each other. Thus we can discuss the conformational difference of the C-terminal domain of mEGF at a side-chain level. As for the N-terminal domain, we cannot discuss the conformation on the basis of the NMR structures.

To identify conformationally different regions in the C-terminal domain, the averages of RMSD per residue around the mean structures of the counterparts were plotted (Figure 2C for the backbone RMSDs; data not shown for the heavy-atom RMSDs). In addition to the two terminal regions, a large difference is seen for residues 47–50, which corresponds to a different running of the backbone chain and a different orientation of the side chains in this region (Figure 6). In Table III we summarize NOE constraints responsible for the structural difference in this region. It is important to show that the NOEs listed in Table III are primarily responsible

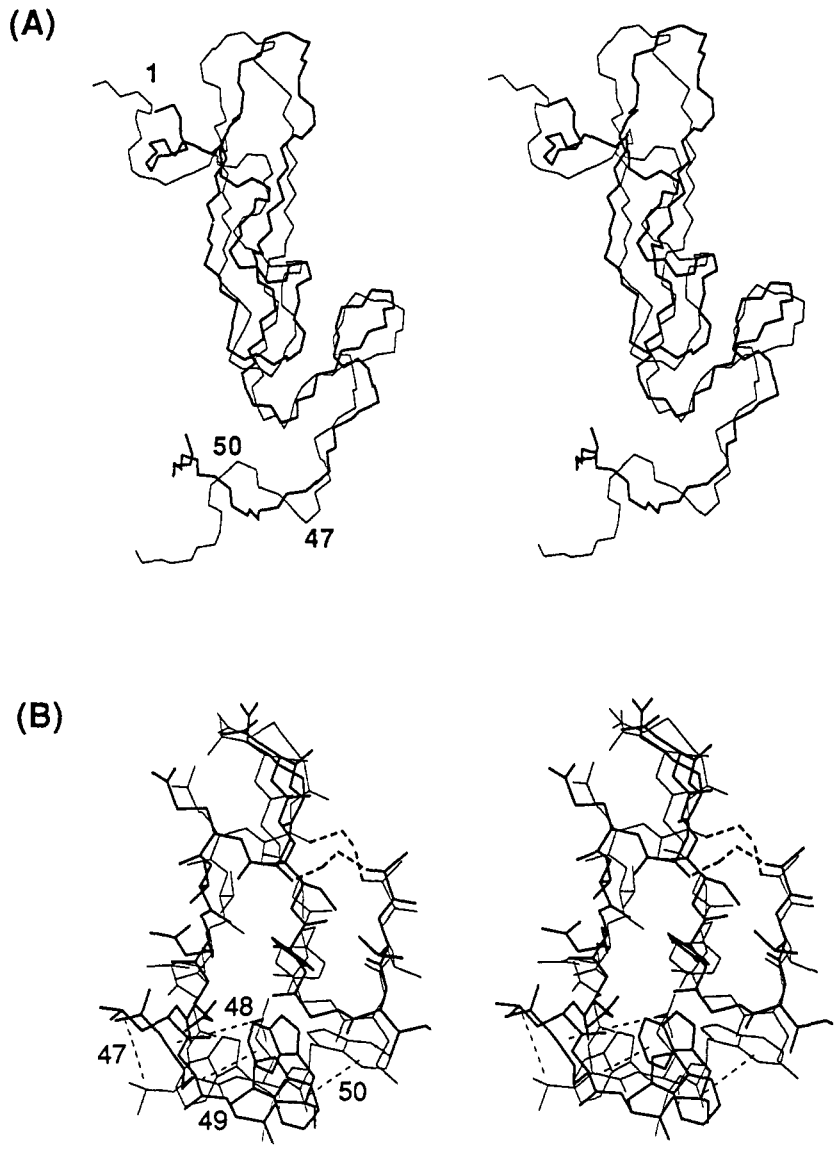

FIGURE 6: (A) Stereoview of a superposition of the backbone atoms of the mean structures at pH 2.0 (thin lines) and that at pH 6.8 (thick lines), best-fitted for the backbone atoms of residues 2–22 + 29–50. One Angstrom unit corresponds to 1.75 mm. (B) Same as (A) for the heavy atoms of the C-terminal domain, residues 33–50, best-fitted for the heavy atoms of residues 33–46 from the same view as Figure 4B. The disulfide bonds are drawn in broken thick lines. The residues of the two structures are connected by broken thin lines for Leu47, Arg48, Trp49, and Trp50. One Angstrom unit corresponds to 2.45 mm.

Table III: NOEs That Make Differences in Conformation of the C-Terminal Tail Region of mEGF[a]

pH 2.0	pH 6.8
I35 HG1#–W49 HN	I35 HG2#–W49 HH2
G36 HA#–W50 HN	G36 HA#–W49 HD1
Y37 HD#–W49 HB#	Y37 HB#–W49 HD1
Y37 HE#–W49 HB#	Y37 HE#–W50 HZ2
Y37 HE#–W49 HZ2	L47 HA–W50 HZ2
R45 HA–W50 HE1	R48 HD#–W50 HH2
R45 HG#–W50 HD1	R48 HD#–W50 HZ2
L47 HA–W50 HZ3	W49 HE3–W50 HB#
W49 HA–W50 HN	W49 HZ3–W50 HA
W49 HB#–W50 HN	W50 HD1–E51 HB#
W49 HE1–W50 HD1	W50 HZ3–E51 HA

[a] # is a "wild-card" character that matches any number.

for the structural differences in the calculated structures. In other words, the structures at pH 2.0 or 6.8 do not satisfy the two NOE sets equally. In fact, the average of RMS NOE violations increases from 0.113 ± 0.003 Å (against the NOE set at pH 2.0) to 0.696 ± 0.053 Å (against the NOE set at pH 6.8) in the case of the 10 structures at pH 2.0. For the five structures at pH 6.8, the average of RMS NOE violations changes from 0.124 ± 0.002 Å (against the NOE set at pH 6.8) to 1.03 ± 0.15 Å (against the NOE set at pH 2.0). The large differences in NOE violations against the cognate and noncognate NOE sets indicate that the structural differences seen in the calculated structures are not an incidental result from the structural calculations. Then we examined distributions of these NOE deviations along the primary sequence (Figure 7). For the pH 2.0 structures, large violations are seen in the C-terminal tail region. For the pH 6.8 structures, large violations are also located in the C-terminal region, though it is less obvious. Note that large violations at residues 22, 24, and 27 in the pH 6.8 structure are due to the lack of NOEs involving these residues at pH 6.8. The large NOE violations in the C-terminal tail region demonstrate that NOEs listed in Table III are responsible for the structural difference in the C-terminal tail region. Figure 6B shows the superposition of the C-terminal domain of the mean structures at pH 2.0 and 6.8 fitted for the heavy atoms of residues 33–46. We excluded residues 47–50 in the fitting process because the segment Arg48–Trp50 was found to be involved in the conformational change (Figures 2C and 7). As readily

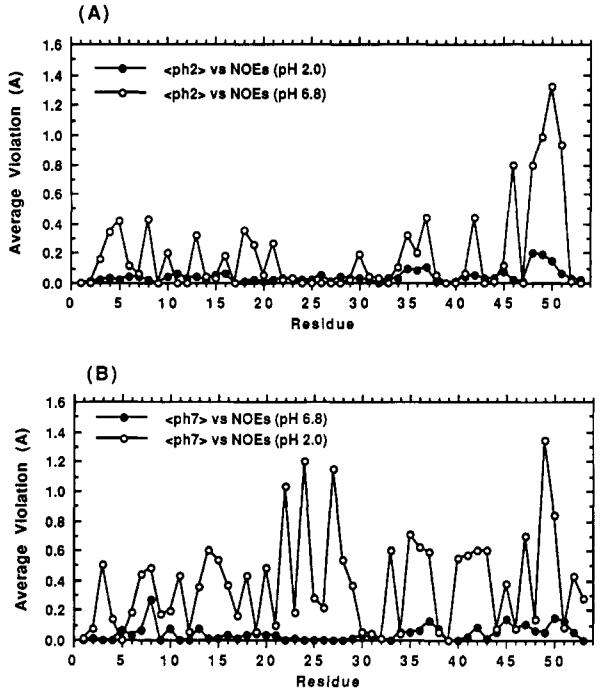

FIGURE 7: Plot of the average values of the NOE violation per residue as a function of residue number (A) for ⟨ph2⟩, the 10 calculated structures at pH 2.0, and (B) for ⟨ph7⟩, the five structures at pH 6.8. The closed circles represent the average violations against the cognate NOE sets, while the open circles are for the noncognate NOE sets.

recognized by inspection of Figure 6B, the running of the backbone and the side-chain orientation of Leu47, Arg48, Trp49, and Trp50 are different between the two pHs.

To discuss conformational difference in the N-terminal domain, we used chemical shifts as a conformational probe. A chemical shift is a more sensitive parameter than NOE for detection of conformational changes in proteins (Folkers et al., 1989). Its nonquantitative nature, however, limits its usefulness to describe protein conformations, so that changes of chemical shifts are only suggestive of conformational changes. For example, proton resonances affected by aromatic rings are much more sensitive than the other resonances. However, due to the high sensitivity of chemical shift, we can expect that no conformational change occurs if we observe no chemical shift changes. Thus, it is safe to conclude whether the conformational change occurs or not when we use many proton resonances as a conformational probe. Bearing this fact in mind, we will interpret the chemical shift differences between the two pHs. Figure 8 shows a comparison between the chemical shifts observed at pH 2.0 and 6.8. The closed bars represent proton resonances of residues having a group that ionizes in the pH range 2–9: Asn1 having an α-amino group; Asp11, Glu24, Asp27, Asp40, Asp46, Glu51, and Arg53 having α-, β-, or γ-carboxyl groups; and His22 having an imidazole group. All these resonances but one (Arg53 $C^{\gamma}H$) move upfield by –0.05 to –0.4 ppm as pH increases. In the N-terminal domain of mEGF, almost all resonances in the residues *without* ionizable groups show shifts as small as +0.05 to –0.1 ppm. These small changes of the chemical shift in the N-terminal domain region demonstrate that the N-terminal domains at the two pHs have nearly identical conformations. Exceptions are Ser8 $C^{\alpha}H$, Tyr13 NH, and Leu26 NH (shown by hatched bars). Because these resonances are isolated in the three-dimensional structure, a local conformational change is unlikely. Ionizable groups found within 3–6 Å suggest direct electrostatic effects: Ser8 $C^{\alpha}H$ and Tyr13 NH were affected by the deprotonation of Asp11, and Leu26 NH by Glu24 and/or Asp27. On the other hand, in the C-terminal domain, the shift of Gln43 $N^{\epsilon'}H$ is interpretable as the direct effect of deprotonation of Asp40. By contrast, the peptide segment Arg48-Trp49-Trp50 includes many of the greatly shifted resonances: Arg48 NH, $C^{\beta}H$, and $C^{\beta'}H$, Trp49 N1H, C2H, C4H, and C5H, and Trp50 NH, $C^{\beta'}H$, C2H, and C4H. These shifts might be a reflection of large ring current shifts of aromatic rings of W49 and W50, but we interpret these shifts as further supporting evidence for the conformational change in this region revealed by the NOE-based calculations. A trigger of the conformational change may be the deprotonation of a carboxyl group. We infer Asp46 as a candidate from the inspection of the three-dimensional structure, but we do not rule out the possibility of Glu51 and the C-terminal α-carboxyl group.

The present three-dimensional structure of mEGF at pH 2.0 calculated with a simulated annealing method (XPLOR) is roughly similar to that of mEGF calculated with the variable target function method (DISMAN) (Montelione et al., 1987) and that of human EGF calculated with a hybrid of distance

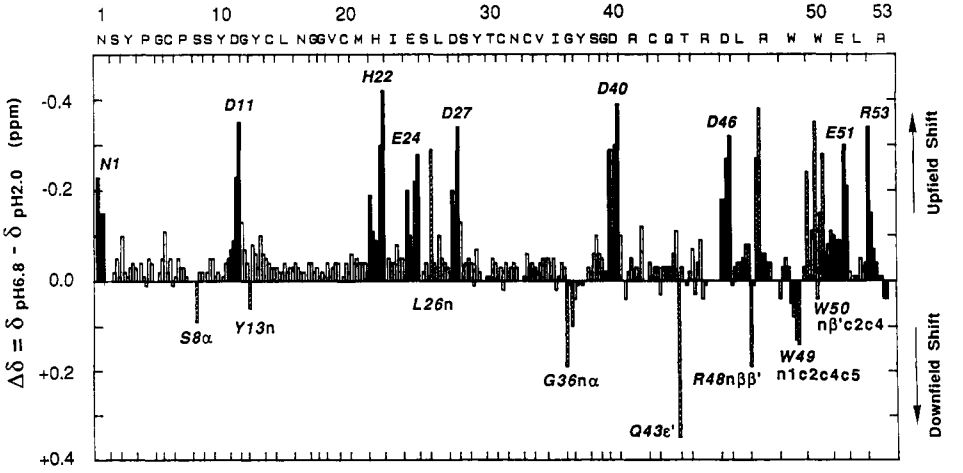

FIGURE 8: Comparison between the chemical shifts of the proton resonances of mEGF at pH 6.8 and 2.0. All proton resonances are aligned along the amino acid sequence and within residues in the following order: NH, α, β, γ, δ,.... Where either resonance in the two states is not observed, no comparison is made and a space is inserted. Closed bars represent the resonances of residues having ionizable groups. Hatched bars represents the resonances having no ionizable groups and of which the chemical shift shifts upfield over 0.15 ppm or downfield over 0.05 ppm. n, α, β, β', and ϵ' denote NH, $C^{\alpha}H$, $C^{\beta}H$, $C^{\beta'}H$, and $C^{\epsilon'}H$, respectively. n1, c2, c4, and c5 denote N1H, C2H, C4H, and C5H, respectively, of a tryptophan residue.

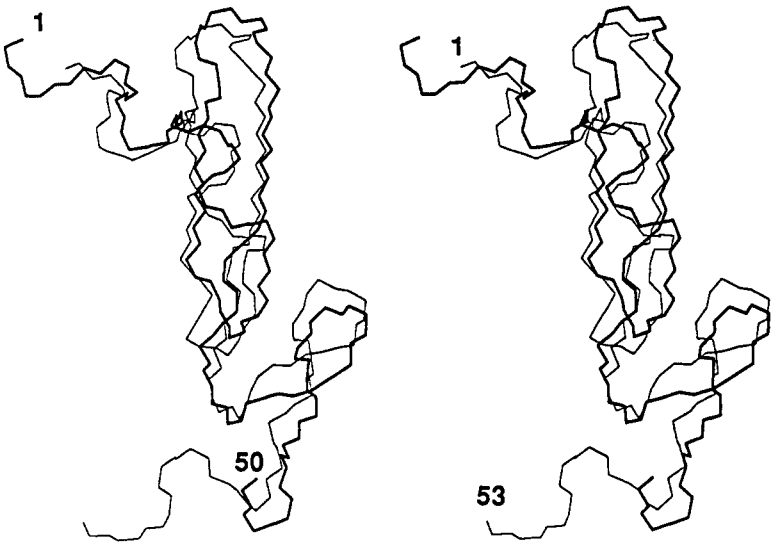

FIGURE 9: Stereoview of a superposition of the backbone atoms of human TGFα (thick lines, model 1 of 4TGF in the Brookhaven Protein Data Bank) and mEGF (thin lines, the mean structure at pH 2.0), best-fitted for the backbone atoms of residues 4–9 + 15–47 of hTGFα and the corresponding residues 2–7 + 13–16 + 18–46 of mEGF. One Angstrom unit corresponds to 1.75 mm.

geometry and restrained molecular dynamics (DISGEO + GROMOS) (Cooke et al., 1987), but these previous structure determinations were rather preliminary. Our present result is much more refined. In the final stage of the preparation of this paper, Montelione et al. (1992) have published the refined structure of mEGF at pH 3.1. Their structure is based on 698 distance constraints and 32 torsion angle constraints. They have also reported the stereospecific assignments of seven β-methylene, four side-chain amide, and one isopropyl methyl protons. Starting from 200 randomly generated initial structures, they obtained 16 final structures with the program DISMAN and subjected the 16 structures to energy minimization. Their structures are almost identical to ours at pH 2.0 as judging from the published stereodiagrams. Their structural convergence is a little worse although they used about twice number of the distance constraints and the stereospecific assignments. Particularly, the convergence of the C-terminal domain is worse in the Montelione structure. Averages of RMSDs for the three backbone atoms and all pairwise combinations are as follows: 1.01 vs. 0.93 Å for residues 1–33, 1.14 vs 0.42 Å for residues 32–47, 1.33 vs 1.19 Å for residues 1–47, and 1.90 vs 1.28 Å for residues 1–50 for Montelione's 16 structures vs our 10 structures at pH 2.0. Detailed comparison of our structures to Montelione's must await the coordinates in the public domain, which will produce interesting results.

TGFα is a 50-residue protein with sequence similarity to EGF. Kline et al. (1990) published the structure of human TGFα at pH 6.3 calculated with a combination of DSPACE with AMBER or XPLOR, and Harvey et al. (1991) reported the structure at pH 6.5 calculated with a combination of GROMOS with DISMAN or DISGEO. Their structures confirm the previously described structures based on a qualitative interpretation of NMR data[3] (Brown et al., 1989; Kohda et al., 1989; Montelione et al., 1989; Tappin et al., 1989). The coordinates of Kline's four structures are now available as 4TGF in the Brookhaven Protein Data Bank. When compared with the structure of mEGF at pH 2.0, model 1 gives the best superposition among the four TGFα structures; RMSD 1.5 Å for the backbone atoms of residues 4–9 + 15–47 of hTGFα and the corresponding residues of mEGF. Figure 9 shows a superposition of hTGFα model 1 and mEGF. They are surprisingly similar to each other. This is consistent with the competitive binding of EGF and TGFα to the same receptor. A plot of average RMSD per residue shows that the N-terminal domains of the two proteins are more similar to each other than the C-terminal domains (data not shown).

In conclusion, we determined the three-dimensional structure of mEGF in neutral pH solution and compared it with the structure in acidic pH solution. The topology of the backbone fold is identical at acidic and neutral pHs (Figure 3). The conformation including the side chains are nearly identical except for the C-terminal tail residues, 47–50 (Figure 6A). This region contains Leu47 that is important in receptor recognition (Ray et al., 1988; Lazer et al., 1988; Engler et al., 1988, Dudgeon et al., 1990; Matsunami et al., 1990). Hence it is reasonable that Leu47 is one of the residues whose conformation is different at the two pHs (Figure 6B). The rearrangement in the C-terminal tail region may be related to the binding ability of EGF to the EGF receptor molecules.

Finally, we would like to emphasize here the importance of the structure determination under physiological conditions, although NMR investigators prefer acidic pHs in order to observe amide protons. Detailed analysis of chemical shifts supplements the loss of information due to the lack of some amide protons. The final purpose of our mEGF investigation is to understand the interaction of EGF with the EGF receptor. The determination of the three-dimensional structure of mEGF at pH 6.8 is a key step for this goal. We have deposited the coordinates of the structures at both pHs in the Brookhaven Protein Data Bank (entries 1EPG, 1EPH, 1EPI, and 1EPJ).

SUPPLEMENTARY MATERIAL AVAILABLE

Three tables (SI, SII, and SIII), containing chemical shifts of mouse EGF at pH 6.8, and constraints used in the calculations for pH 2.0 and 6.8, and four figures (S1, S2, S3, and S4), containing the distance map, superpositions of the backbone structure of each domain, and Ramachandran plots for total residues and each residue at pH 2.0 and 6.8 (21 pages). Ordering information is given on any current masthead page.

[3] Some disagreement in the structures of human TGFα from different researchers is due to the different pHs used, as pointed out by Harvey et al. (1991). TGFα exists in multiple conformational states at low pH (Tappin et al., 1989).

REFERENCES

Bax, A., & Davis, D. G. (1985) *J. Magn. Reson. 65*, 393–402.
Braun, W., & Go, N. (1985) *J. Mol. Biol. 186*, 611–626.
Brooks, B. R., Bruccoleri, R. E., Olafson, B. D., States, D. J., Swaminathan, S., & Karplus, M. (1983) *J. Comput. Chem. 4*, 187–217.
Brown, S. C., Müller, L., & Jeffs, P. W. (1989) *Biochemistry 28*, 593–599.
Brünger, A. T. (1990) XPLOR Softward Manual, version 2.1, Yale University, New Haven, CT.
Carpenter, G., & Cohen, S. (1979) *Annu. Rev. Biochem. 48*, 193–216.
Carpenter, G., & Cohen, S. (1990) *J. Biol. Chem. 265*, 7709–7712.
Carver, J. A., Cooke, R. M., Esposito, G., Campbell, I. D., Gregory, H., & Sheard, B. (1986) *FEBS Lett. 205*, 77–81.
Clore, G. M., Brünger, A. T., Karplus, M., & Gronenborn, A. M. (1986) *J. Mol. Biol. 191*, 523–551.
Clore, G. M., Nilges, M., & Ryan, C. A. (1987) *Biochemistry 26*, 8012–8023.
Cooke, R. M., Wilkinson, A. J., Baron, M., Pastore, A., Tappin, M. J., Campbell, I. D., Gregory, H., & Sheard, B. (1987) *Nature 327*, 339–341.
Cooke, R. M., Tappin, M. J., Campbell, I. D., Kohda, D., Miyake, T., Fuwa, T., Miyazawa, T., & Inagaki, F. (1990) *Eur. J. Biochem. 193*, 807–815.
Dudgeon, T. J., Cooke, R. M., Baron, M., Campbell, I. D., Edwards, R. M., & Fallon, A. (1990) *FEBS Lett. 261*, 392–396.
Engler, D. A., Matsunami, R. K., Campion, S. R., Stringer, C. D., Stevens, A., & Niyogi, S. K. (1988) *J. Biol. Chem. 263*, 12384–12390.
Folkers, P. J. M., Clore,G. M., Driscoll, P. C., Dodt, J., Köhler, S., & Gronenborn, A. M. (1989) *Biochemistry 28*, 2601–2617.
Greenfield, C., Hiles, I., Waterfield, M. D., Federwisch, M., Wollmer, A., Blundell, T. L., & McDonald, N. (1989) *EMBO J. 8*, 4115–4123.
Havel, T. F., & Wüthrich, K. (1985) *J. Mol. Biol. 182*, 281–294.
Harvey, T. S., Wilkinson, A. J., Tappin, M. J., Cooke, R. M., & Campbell, I. D. (1991) *Eur. J. Biochem. 198*, 555–562.
Holladay, L. A., Savage, C. R., Jr., Cohen, S., & Puett, D. (1976) *Biochemistry 15*, 2624–2633.
Honegger, A. M., Schmidt, A., Ullrich, A., & Schlessinger, J. (1990) *Mol. Cell. Biol. 10*, 4035–4044.
Jeener, J., Meier, B. H., Bachmann, P., & Ernst, R. R. (1979) *J. Chem. Phys. 71*, 4546–4553.
Kline, A. D., Braun, W., & Wüthrich, K. (1988) *J. Mol. Biol. 204*, 675–724.
Kline, T. P., Brown, F. K., Brown, S. C., Jeffs, P. W., Kopple, K. D., & Müller, L. (1990) *Biochemistry 29*, 7805–7813.
Kohda, D., & Inagaki, F. (1988) *J. Biochem. (Tokyo) 103*, 554–571.
Kohda, D., Go, N., Hayashi, K., & Inagaki, F. (1988) *J. Biochem. (Tokyo) 103*, 741–743.
Kohda, D., Shimada, I., Miyake, T., Fuwa, T., & Inagaki, F. (1989) *Biochemistry 28*, 953–958.
Kohda, D., Sawada, T., & Inagaki F. (1991) *Biochemistry 30*, 4896–4900.
Kuszewski, J., Nilges, M., & Brünger, A. T. (1992) *J. Biomol. NMR 2*, 33–56.
Lazar, E., Watanabe, S., Dalton, S., & Sporn, M. B. (1988) *Mol. Cell. Biol. 8*, 1247–1252.
Macura, S., Huang, Y., Suter, D., & Ernst, R. R. (1981) *J. Magn. Reson. 43*, 259–281.
Marion, D., & Wüthrich, K. (1983) *Biochem. Biophys. Res. Commun. 113*, 967–974.
Massagué, J. (1983) *J. Biol. Chem. 258*, 13614–13620.
Matrisian, L. M., Planck, S. R., & Magun, B. E. (1984) *J. Biol. Chem. 259*, 3047–3052.
Matsunami, R. K., Campion, S. R., Niyogi, S. K., & Stevens, A. (1990) *FEBS Lett. 264*, 105–108.
Mayo, K. H., Cavalli, R. C., Peters, A. R., Boelens, R., & Kaptein, R. (1989) *Biochem. J. 257*, 197–205.
Metzler, W. J., Hare, D. R., & Pardi, A. (1989) *Biochemistry 28*, 7045–7052.
Montelione, G. T., Wüthrich, K., Nice, E. C., Burgess, A. W., & Scheraga, H. A. (1986) *Proc. Natl. Acad. Sci. U.S.A. 83*, 8594–8598.
Montelione, G. T., Wüthrich, K., Nice, E. C., Burgess, A. W., & Scheraga, H. A. (1987) *Proc. Natl. Acad. Sci. U.S.A. 84*, 5226–5230.
Montelione, G. T., Wüthrich, K., & Scheraga, H. A. (1988) *Biochemistry 27*, 2235–2243.
Montelione, G. T., Winkler, M. E., Burton, L. E., Rinderknecht, E., Sporn, M. B., & Wagner, G. (1989) *Proc. Natl. Acad. Sci. U.S.A. 86*, 1519–1523.
Montelione, G. T., Wüthrich, K., Burgess, A. W., Nice, E. C., Wagner, G., Gibson, K. D., & Scheraga, H. A. (1992) *Biochemistry 31*, 236–249.
Neuhaus, D., Wagner, G., Vasak, M., Kägi, J. H. R., & Wüthrich, K. (1985) *Eur. J. Biochem. 151*, 257–273.
Nilges, M., Clore, G. M., & Gronenborn, A. M. (1988) *FEBS Lett. 229*, 317–324.
Pastan, I. H., & Willingham, M. C. (1981) *Science 214*, 504–509.
Planck, S. R., Finch, J. S., & Magun, B. E. (1984) *J. Biol. Chem. 259*, 3053–3057.
Plateau, P., & Gueron, M. (1982) *J. Am. Chem. Soc. 104*, 7310–7311.
Priestle, J. P. (1988) *J. Appl. Crystallogr. 21*, 572–576.
Ramachandran, G. N., Ramakrishnan, C., & Sasisekharan, V. (1963) *J. Mol. Biol. 7*, 95–99.
Rance, M., Sørensen, O. W., Bodenhausen, G., Wagner, G., Ernst, R. R., & Wüthrich, K. (1983) *Biochem. Biophys. Res. Commun. 117*, 479–485.
Ray, P., Moy, F. J., Montelione, G. T., Liu, J.-F., Narang, S. A., Scheraga, H. A., & Wu, R. (1988) *Biochemistry 27*, 7289–7295.
Richardson, J. S. (1981) *Adv. Protein Chem. 34*, 167–282.
Savage, C. R., Jr., Hash, J. H., & Cohen, S. (1973) *J. Biol. Chem. 248*, 7669–7672.
States, D. J., Haberkorn, R. A., & Reuben, D. J. (1982) *J. Magn. Reson. 48*, 286–292.
Takahashi, S., & Nagayama, K. (1988) *J. Magn. Reson. 76*, 347–351.
Tappin, M. J., Cooke, R. M., Fitton, J. E., & Campbell, I. D. (1989) *Eur. J. Biochem. 179*, 629–637.
Taylor, J. M., Mitchell, W. M., & Cohen, S. (1972) *J. Biol. Chem. 247*, 5928–5934.
Tycko, B., & Maxfield, F. R. (1982) *Cell 28*, 643–651.
Ullrich, A., & Schlessinger, J. (1990) *Cell 61*, 203–212.
van Gunsteren, W. F., & Berendsen, H. J. C. (1982) *Biochem. Soc. Trans. 10*, 301–305.
Wüthrich, K. (1986) in *NMR of Proteins and Nucleic Acids*, John Wiley, New York.
Zuiderweg, E. P. R., Hallenga, K., & Olejniczak, E. T. (1986) *J. Magn. Reson. 70*, 336–343.

Registry No. EGF, 62229-50-9; Leu, 61-90-5.